Cell Reports
Physical Science

CellPress
OPEN ACCESS

Article

Interpreting accelerated tests on perovskite modules using photooxidation of $MAPbI_3$ as an example

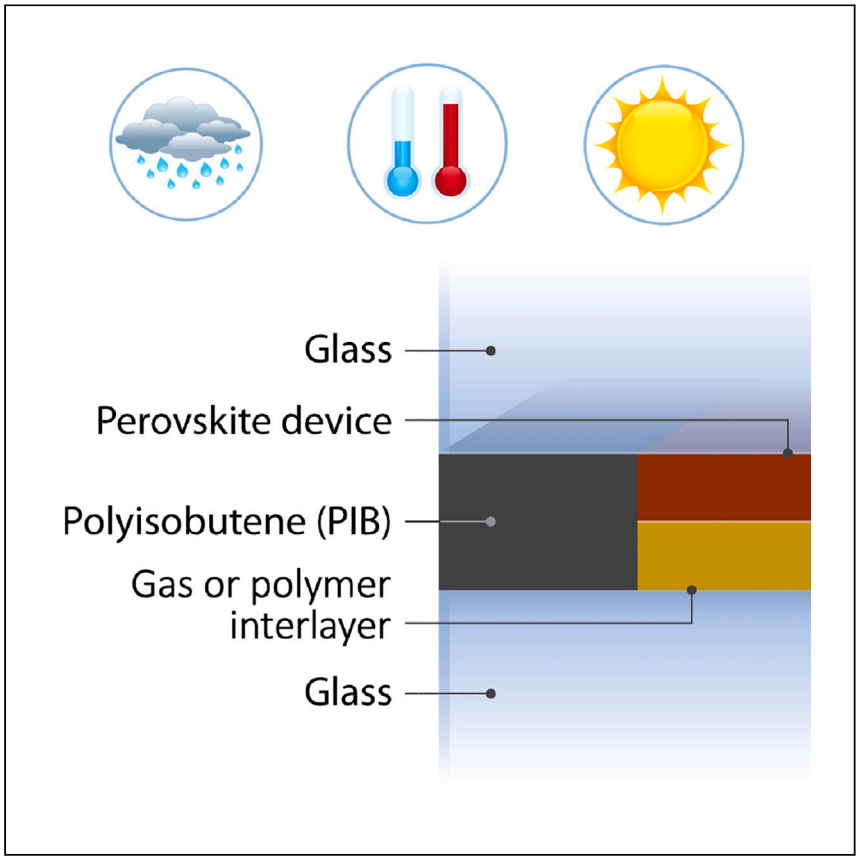

Metal halide perovskite solar cells exhibit impressive power conversion efficiencies and are deposited by a variety of techniques, which has led to expectations of a fast track to commercialization. Here, Repins et al. use a physics and chemistry of failure approach to explore how accelerated tests can create future reliability.

Ingrid L. Repins, Michael Owen-Bellini, Michael D. Kempe, ..., Nutifafa Y. Doumon, Timothy J. Silverman, Laura T. Schelhas

ingrid.repins@nrel.gov

Highlights

Acceleration factors are calculated for perovskite solar panels in stress tests

A physics and chemistry of failure approach is used

Photooxidation of methylammonium lead iodide is used to illustrate the method

Acceleration factors in common accelerated tests are found to be low

Repins et al., Cell Reports Physical Science 5, 101969
May 15, 2024
https://doi.org/10.1016/j.xcrp.2024.101969

Cell Reports
Physical Science

CellPress
OPEN ACCESS

Article

Interpreting accelerated tests on perovskite modules using photooxidation of $MAPbI_3$ as an example

Ingrid L. Repins,[1,5,*] Michael Owen-Bellini,[1] Michael D. Kempe,[1] Michael G. Deceglie,[1] Joseph J. Berry,[1,2,3] Nutifafa Y. Doumon,[1,4] Timothy J. Silverman,[1] and Laura T. Schelhas[1]

SUMMARY

Solar panels (modules) based on metal halide perovskites are following a fast track to commercialization. Unlike more established solar cell materials, there are not yet decades-long field observations to increase consumer confidence. The "physics and chemistry of failure" approach is used in other industries and estimates product degradation based on laboratory accelerated tests integrated with an understanding of degradation mechanisms. This work uses that approach to quantify the relationship between accelerated tests and projected product behavior for metal halide perovskite modules. Degradation involving photooxidation of methylammonium lead iodide is used to illustrate the method. Acceleration factors in common accelerated tests are found to be low. Conclusions emphasize that the accelerated tests on photovoltaics should not be interpreted as equivalent across module types or as a green light for commercialization unless supported by the appropriate field data or physics and chemistry of failure analysis.

INTRODUCTION

Metal halide perovskite (MHP) photovoltaic (PV) devices have exhibited impressive cell efficiencies. Furthermore, these solar absorbers have been deposited via numerous solution and vapor deposition techniques that are viewed as less costly than Si wafer processing for traditional PVs. This combination has led to expectations that MHP solar panels are following a fast track to commercialization.[1–7]

A key consideration in product development is ensuring that MHP modules can be fielded for at least 20 years, like commercially available Si and CdTe modules, both to keep the cost of generated electricity low[8] and to meet customer expectations of warranties.[9] This need for decades-long stability has been identified as a pivotal issue in bringing perovskite technology to commercialization.[10,11] While early champion efficiency MHP solar cells based on methylammonium lead iodide ($MAPbI_3$)[12] degraded significantly with minutes to hours of operation in air,[13,14] researchers have since made substantial progress in developing packaging and stabilizing materials and interfaces.[15–18]

The typical method for evaluating the durability of PV modules involves accelerated tests, i.e., increasing stress levels (such as temperature and humidity) beyond the highest values encountered in the field to speed up degradation and then using behavior from a short test to understand susceptibility to degradation from these stresses in a much longer field deployment. Accelerated tests for Si modules have

[1]National Renewable Energy Laboratory, Golden, CO 80401, USA

[2]Department of Physics, University of Colorado, Boulder, CO 80309, USA

[3]Renewable and Sustainable Energy Institute, University of Colorado, Boulder, CO 80309, USA

[4]Present address: Department of Materials Science and Engineering, The Pennsylvania State University, University Park, PA 16802, USA

[5]Lead contact

*Correspondence: ingrid.repins@nrel.gov

https://doi.org/10.1016/j.xcrp.2024.101969

been developed empirically, using decades of observation to identify degradation mechanisms, important stresses, and appropriate pass-fail criteria in accelerated tests and standards.[19] A seminal study in the development of appropriate accelerated tests for Si modules was the Jet Propulsion Laboratory (JPL) "block buy" program.[20,21] This study, executed from 1975 to 1986, saw lifetimes of Si modules increase from 1 year at the beginning of the study to 10 years by the end.[20] The study involved successive cycles of

(1) Deploying modules outdoors,
(2) Waiting for them to exhibit failures,
(3) Identifying stresses likely to induce those failures in a test environment (e.g., applying heat and humidity might reproduce observed metal corrosion),
(4) Writing an accelerated test protocol to reproduce the observed failure,
(5) Purchasing improved modules that could pass those tests, and then
(6) Returning to step 1 with the improved modules.

This process was successful at identifying failure modes in Si modules and defining accelerated tests to reproduce them, as evidenced not only by the increase in module lifetime to >10 years over the course study but also by the recent documentation of systems from that era exceeding 30 years of operation.[22–24] The earliest surviving PV arrays based on CdTe or $CuIn_xGa_{1-x}Se_2$ (CIGS) are also now approaching 30 years of field observation.[25] Standard warranties for existing products are around 25 years, and decades-long performance and stability have a strong effect on the cost of generated electricity[26] and the value of the module.[27]

Understandably, optimism for commercial readiness increased when MHP test articles passed some accelerated tests typically used in commercial product design qualification.[28–31] However, even experienced stakeholders may misinterpret that the results of such tests on MHP prototypes "allow for their commercial development."[32] Caution in the interpretation of early test results is warranted because MHP modules will have unique degradation mechanisms that are accelerated differently than those in Si or CdTe.

For a given technology, how a degradation mechanism responds to a certain stress condition is captured by the acceleration factor (AF). For a given degradation mechanism and accelerated test, it is defined as

$$AF = \frac{\text{time in field to achieve a given degradation from this mechanism}}{\text{time in test to achieve the same degradation from this mechanism}}. \quad \text{(Equation 1)}$$

The AF is specific to each degradation mechanism and technology. A given test can result in different AFs for different technologies. For example, the potential-induced degradation test in IEC 61215 was found to have an AF of 2,000 for Si modules,[33] 395 for CIGS modules mounted using clips with standard rubber,[34] and 23 for CIGS modules mounted using clips with high-resistivity rubber.[34] Thus, to interpret whether passing a design qualification test means that a product is ready for market, we must understand what the relevant failure mechanisms are, and whether they are adequately accelerated by the test to probe the desired product lifetime, as a function of both the solar cell and the packaging used.

Tests with known AFs for a given product type can provide customer confidence in reaching the expected fielded lifetime. In contrast, tests without known AFs tend to provide only a relative comparison (i.e., formulation A is more stable than formulation B).

Deriving AFs is particularly important for risk reduction in MHP-based modules compared to modules based on other absorbers (e.g., Si or CdTe) due to the desire for rapid commercialization and lack of multi-decade MHP field demonstrations. Some examinations of perovskite test articles outdoors have begun,[35–42] and other studies have compared such observations with accelerated tests[43] or provided predictions of behavior based on empirical fits to accelerated test data.[15] However, established AFs for MHP devices are lacking due to the short history of outdoor exposure (compared to the desired product lifetime) and incomplete knowledge of the relevant degradation mechanisms. In other words, it is unknown whether the important degradation mechanisms that may occur over decades have been identified, and for each mechanism, the number to put in the numerator in Equation 1 is unknown.

Predicting decades of performance behavior without decades of field observation thus requires utilizing the physics and chemistry of failure.[9] This approach involves (1) using field observation or test-to-failure to identify degradation mechanisms and stresses that accelerate them; (2) for each degradation mechanism, hypothesizing physics- and chemistry-based models that relate stress level and time to degradation amount; (3) evaluating and validating these relationships with experimental data; (4) evaluating models with inputs that represent the desired use environments; and (5) predicting longer-term fielded behavior. The need to use a physics of failure approach is encountered in other industries where technology changes quickly. For example, in the integrated circuit industry, as in PVs, standards for product qualification have been developed empirically and typically involve fixed stress exposures. However, a compressed product development cycle introducing new technology, or a requirement to predict product lifetime more quantitatively, can benefit from the incorporation of a physics and chemistry of failure approach.[44,45]

In this work, we use a physics and chemistry of failure approach to calculate the AF for some accelerated tests that are commonly used on MHP. There are many different compositions of MHP absorbers, with different chemical considerations that can lead to different primary degradation mechanisms. In this work, we analyze the most well-studied MHP absorber for which the primary degradation mechanism is relatively well characterized—photooxidation of $MAPbI_3$.[46] While there are more modern formulations of MHPs topping the efficiency charts, using $MAPbI_3$ provides a useful case study to illustrate the necessary information and methods for calculating AF in this and other MHP structures. The analysis indicates that, for this degradation mechanism, more rigorous accelerated testing of $MAPbI_3$ is needed to produce results that probe the timescale of the expected product lifetime.

We focus specifically on dry photooxidation (DPO) of $MAPbI_3$ because the relationship between test and field conditions for water ingress through desiccant-filled PIB (polyisobutene) has already been documented thoroughly in other publications[47–50] aimed at applications in CdTe or CIGS modules. However, the impact of O_2 in MHPs differs from that in chalcogenides. In MHPs, O_2 causes degradation, whereas, in chalcogenides, O_2 is isovalent with the chalcogen anion and improves device performance.[51,52] Thus, in this work, we focus on O_2 ingress, which is not absorbed by the desiccant in a traditional edge seal and has not been studied for earlier types of thin-film modules.

RESULTS AND DISCUSSION

Methodology

We utilize a two-step model where O_2 diffuses into the module package and then photooxidizes the MHP at a rate that is dependent on the local O_2 concentration,

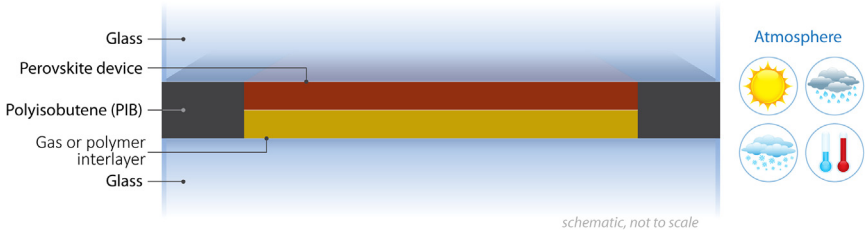

Figure 1. Schematic of module package used to calculate diffusion and reaction
Gases will diffuse through the PIB (shown in black) into the interlayer (shown in yellow) and eventually into the device (shown in red).

temperature, and free electron concentration. We use experimentally derived, published diffusion-related and kinetic constants. While this paper performs such predictions for one degradation mechanism, the physics and chemistry of failure approach can be applied more widely as degradation modes for new cell and module types are identified and degradation kinetics are quantified.

To estimate the change in MHP performance over time, the O_2 concentration within the module from diffusion through the edge seal[53] is coupled with the kinetics for the absorber photooxidation[46] and the resulting photon absorption loss. The structure used for calculation is shown in Figure 1 and is similar to the package used by commercial CdTe modules[54] and some perovskite test articles.[17] A glass top sheet and back sheet are sealed around the perimeter by a desiccant-filled PIB edge seal that is 1 cm wide (in the direction of O_2 ingress) and 450 μm thick. These edge seal dimensions are typical for commercial CIGS and CdTe modules. The interior of the module consists of two layers: an MHP device stack with a solar absorber that is $\leq$2 μm thick and a polymer or inert gas interlayer that fills the area behind the solar cell. The module size was chosen as 1 × 2 m, similar to current thin-film products.

Diffusion model

For the O_2 diffusion portion of the model, we assume Fickian diffusion, i.e.,

$$\frac{\partial C}{\partial t} = D\,\nabla^2 C, \qquad \text{(Equation 2)}$$

where C is the concentration of O_2 in the solid, D is the diffusivity, and t is the time. Surface concentrations are taken to be consistent with Henry's law. Thus, at a gas-solid interface,

$$P = \frac{C}{S}, \qquad \text{(Equation 3)}$$

where P is the partial pressure of the diffusing species, C is the concentration of the diffusing species within the solid at the gas-solid interface, and S is the solubility of the diffusing species in the solid.

At an interface between two solids (1 and 2),

$$\frac{C_1}{S_1} = \frac{C_2}{S_2}. \qquad \text{(Equation 4)}$$

The concentration may be discontinuous at the interface: C_1 and C_2 are the concentrations at the interface but on the solid 1 or solid 2 side of the interface, respectively. Solubility and diffusivity are a function of temperature, T, in the typical form

$$D = D_0 \cdot e^{\frac{-Ead}{T}} \qquad \text{(Equation 5)}$$

$$S = S_0 e^{-Eas/T}. \quad \text{(Equation 6)}$$

Values for the activation energies (E_{ad}, E_{as}), prefactors (D_0, S_0), and other properties needed for calculations are taken from the literature and documented in Table S1. Published properties of PIB are listed under the brand name "Oppanol."[53] The format of Equations 2, 3, 4, 5, and 6 are the same as those used in widely applied, well-known expressions[55,56] for the water vapor transmission rate (WVTR) in solar modules[47,57,58] and other barriers.[59,60]

In this work, we assume that O_2 is evenly distributed in the interlayer, and Equation 2 then reduces to a single dimension in the edge seal. The accuracy of this assumption for a given packaging type depends on the relative diffusivities and widths of the edge seal and interlayer. For modules utilizing an inert gas as the interlayer,[61–63] uniform O_2 distribution is always a valid assumption because the self-diffusivity of O_2 in N_2[64] is $\sim 10^6$ times greater than that in PIB. In a different example, the diffusivity of O_2 in typical polymer encapsulants is $\sim$10 times greater[65,66] than that in PIB. Thus, cells or mini-modules packaged with a PIB edge seal and polymer interlayer (for example, Toniolo[67] or Cheacharoen[68]) are well approximated by uniform O_2 distribution in the interlayer, but a large module is expected to exhibit non-negligible deviations from the simplified approximation.

In this study, we encounter the unique situation where the concentration of the diffusing species in the module interlayer varies with time, depending on how much O_2 has diffused through the desiccant-filled PIB edge seal and how much O_2 has been consumed by the MHP. A further boundary condition based on the conservation of mass is thus required:

$$\text{moles } O_2 \text{ flowed into the interlayer} = \text{moles in the interlayer} + \text{moles consumed by the MHP}, \quad \text{(Equation 7)}$$

which can be stated mathematically as

$$A_{PIB}\int_0^t -D\frac{dC_{PIB}}{dx}\,dt\Big|^{x \text{ at PIB inner edge}} = C_{interlayer}V_{interlayer} + \frac{1}{4}A_{MHP}\int_0^t rate_{MHP}\,dt, \quad \text{(Equation 8)}$$

where A_{PIB} is the area of the entire PIB edge seal perpendicular to the diffusion direction, $V_{interlayer}$ is the volume of the interlayer, A_{MHP} is the surface area of the MHP film, and $rate_{MHP}$ is the surface reaction rate[46] between MHP and O_2. The factor of $^1/_4$ in the rate term occurs because each mole of O_2 consumes 4 mol of MHP.[69]

Oxidation model

The rate of MHP oxidation as a function of exposure conditions is taken from work by Siegler et al.[46] The expression for the rate of DPO is

$$rate_{MHP} = k_{0,DPO}\, e^{-E^{eff}_{A,DPO}/k_BT}\, \frac{P_{O2}\, I_{in}^{0.7}}{1+K_{2D}\, P_{O2}\left(1+K_{3D}\, I_{in}^{0.7}\right)}. \quad \text{(Equation 9)}$$

This expression yields a rate for a surface reaction (moles oxidized per cm^2 of film area per s). The constants $k_{0,DPO}$, $E^{eff}_{A,DPO}$, K_{2D}, and K_{3D} are constants derived from experiment in Kempe et al.[46] P_{O2} relates to the output of the diffusion portion of the simulation (Equations 2, 3, 4, 5, and 6). The quantities k_BT and I_{in} relate to the exposure variables temperature and free carrier density, respectively. I_{in} is included in the rate equation because the reaction requires a free electron.[70] I_{in} is given in terms of the experimental incident flux of photons with energy greater than the band gap for a film of fixed thickness,[46] t_{film}. In a module or solar cell, excess carrier

density also depends on the voltage operating point, not just the incident photon flux. To relate these two quantities, we approximate for a film[71]

$$\Delta n \approx \tau\ (I_{in}\ /\ t_{film}), \qquad \text{(Equation 10)}$$

where τ is the minority carrier lifetime and Δn is the excess carrier concentration. An estimate of cell or module Δn at a given operating point thus allows approximating the equivalent I_{in} to use as an input in Equation 9.

Performance model

Device performance is impacted by decreasing absorption as MHP is lost to photooxidation, essentially decreasing the effective film thickness,[46,72] ℓ, according to

$$\ell(t) = \ell(0) - \frac{W}{\rho}\int rate_{MHP}(t)dt, \qquad \text{(Equation 11)}$$

where W is the MHP molar mass and ρ is the density. The time at which testing starts and the module package is first exposed to O_2 is defined to be $t = 0$.

If the AM1.5 global spectrum is expressed in terms of photons per wavelength per second, then the fraction of photons transmitted through the film, f_T, is

$$f_T(t) = \frac{\int_{\frac{hc}{\lambda} > E_g} AM1.5(\lambda)e^{-\alpha(\lambda)\ell(t)}d\lambda}{\int_{\frac{hc}{\lambda} > E_g} AM1.5(\lambda)d\lambda}. \qquad \text{(Equation 12)}$$

Absorption data α are taken from the literature.[73] The integral in Equation 12 proceeds only for photons with energy $\left(\frac{hc}{\lambda}\right)$ greater than the band gap E_g. Approximating that the short-circuit current J_{sc} is proportional to the number of absorbed photons,

$$\frac{J_{sc}(t)}{J_{sc}(0)} \approx \frac{1 - \frac{\int_{\frac{hc}{\lambda} > E_g} AM1.5(\lambda)e^{-\alpha(\lambda)\ell(t)}d\lambda}{\int_{\frac{hc}{\lambda} > E_g} AM1.5(\lambda)d\lambda}}{1 - \frac{\int_{\frac{hc}{\lambda} > E_g} AM1.5(\lambda)e^{-\alpha(\lambda)\ell(0)}d\lambda}{\int_{\frac{hc}{\lambda} > E_g} AM1.5(\lambda)d\lambda}} \approx \frac{P(t)}{P(0)}. \qquad \text{(Equation 13)}$$

Equation 13 also includes an expression for the fraction of power retained at any time, as it is assumed that current loss is the dominant performance consequence of photooxidation. This assumption is consistent with experiment,[72] though it is a conservative estimate of degradation because it does not account for possible simultaneous decrease of the fill factor.

Numerical calculations using Equations 1, 2, 3, 4, 5, 6, 7, 8, 9, 10, 11, 12, and 13 were performed. The subsections below examine results, building in complexity from concentration profiles and associated lag times, to performance degradation and resulting AFs, to limiting cases and the implications for packaging and flow.

Lag times

Concentration profiles indicate that DPO of packaged $MAPbI_3$ will initially be slow due to two lag times. The first lag time occurs because O_2 does not penetrate the PIB immediately, as shown in Figure 2. In this example, calculated for 75°C test conditions, the solubility of O_2 in PIB allows little O_2 to reach the module interior during the first day of exposure. This trend can be seen by examining the spatial

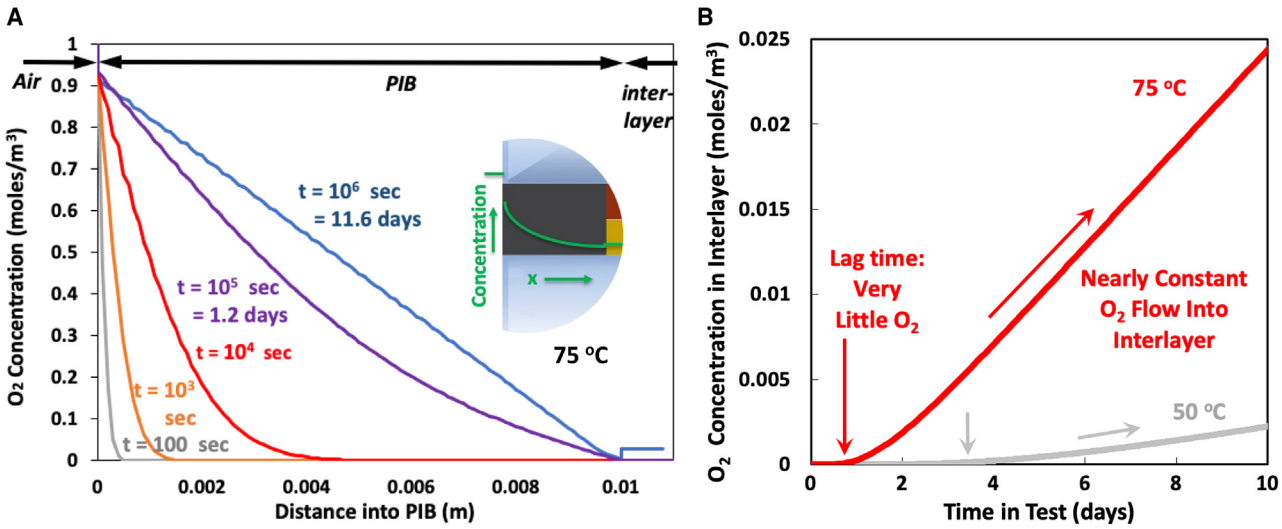

Figure 2. Illustration of lag time in O_2 diffusion through PIB at 75°C

(A) Calculated O_2 concentration as a function of distance into PIB at five different times. The inset shows, in green lines, the region of the structure described by (A).

(B) O_2 concentration in the interlayer as a function of time, shown at both 75°C and 50°C. Arrows mark lag times and constant flow regions.

concentration profile of O_2 in the PIB (Figure 2A) or the cumulative concentration of O_2 in the interlayer as a function of time (Figure 2B). In general, lag times and flow rates are a function of temperature. In Figure 2B, the cumulative O_2 concentration is also shown at both 75°C and 50°C. Both curves are qualitatively similar, but the lag time is longer and the flow is slower when temperature is reduced.

A second lag time occurs related to device performance. In a thick absorber, a small change in thickness due to oxidation has little effect on overall absorption and short-circuit current. Thus, power degradation is initially slow—even if the MHP is being consumed quickly—and speeds up as the absorber becomes optically thin. The net effect of these two lag times is that a short accelerated test results in very little degradation.

AFs for several test conditions

Expected degradation due to photooxidation of $MAPbI_3$ was calculated for several relevant or common test conditions, which are summarized in Table 1. These conditions include an approximation of fielded exposure in a temperate climate ("fielded"), fielded exposure omitting the nighttime conditions ("always day"), light and heat test,[74] ISOS-L-2 at 65°C,[75] ISOS-L-2 at 85°C,[75] and the IEC 61215 damp heat test (MQT 13).[76] "Fielded" conditions are approximated by an 8 h daytime condition, where temperature is mildly elevated (50°C) and the voltage operating point is non-zero. The remaining 16 h of the day are nighttime conditions, which are cooler and without voltage. The operating point is important to the photooxidation rate, as the reaction requires a free electron.[70] Simulation inputs associated with the test protocols of Table 1 are graphed as a function of time in Figure 3.

The AFs in the rightmost column of Table 1 are derived from Figure 4, which shows the evolution of power output for each test condition. Each curve in Figure 4 results from a numerical solution of Equations 2, 3, 4, 5, 6, 7, 8, 9, 10, 11, 12, and 13, with the temperatures and excess carrier densities input according to Figure 3. The results in Figure 4 are shown for two different $MAPbI_3$ thicknesses. AFs were calculated by

Table 1. Accelerated test conditions and resulting AFs calculated in this study

	Temperature (°C)		Operating point		
Condition	8 h per day	16 h per day	8 h per day	16 h per day	Resulting AF
Fielded	50	25	maximum power	dark	1
Always day	50	50	maximum power	maximum power	2
Light and heat	75	75	short circuit	short circuit	3
ISOS-L-2 65	65	65	maximum power	dark	4
ISOS-L-2 85	85	85	maximum power	dark	10
IEC 61215 DH	85	85	dark	dark	0

comparing the time to reach 80% of the initial power under each test condition to that for the fielded condition. Several conclusions can be drawn from Figure 4.

(1) AFs are low. Even the most aggressive condition in Table 1 can only screen for early failures. In contrast, some degradation mechanisms in Si modules can be induced with a much higher AF. For example, commonly used test conditions for potential-induced degradation shunting have been shown to produce an AF of 2,000.[33] Thermal cycling to test solder bond fatigue produces an AF of around 500.[77]

(2) Neither wet photooxidation nor DPO of $MAPbI_3$ can occur without charge carriers. Thus, IEC 61215-2 MQT 13 (red line in Figure 4), and dark tests in general, is not expected to accelerate the primary degradation mode for $MAPbI_3$. The excess carrier density in the dark is orders of magnitude lower than that encountered at maximum power or open-circuit operating points.

(3) The power degradation rate for DPO depends on film thickness, but AFs are approximately (within 10%) independent of thickness for a given test condition.

(4) Temperature is the most important variable differentiating the test conditions. For either film thickness, the degradation curves are ordered from left to right approximately in order of decreasing average temperature. There are two exceptions to the ordering, both related to excess carrier density. In the fully dark case, the degradation rate is limited almost to zero because the free carrier density is very low—nearly six orders of magnitude lower than that at the maximum power voltage, V_{mp}. For the light and heat test condition, at short circuit, the carrier density is ~100× lower than at V_{mp}, which

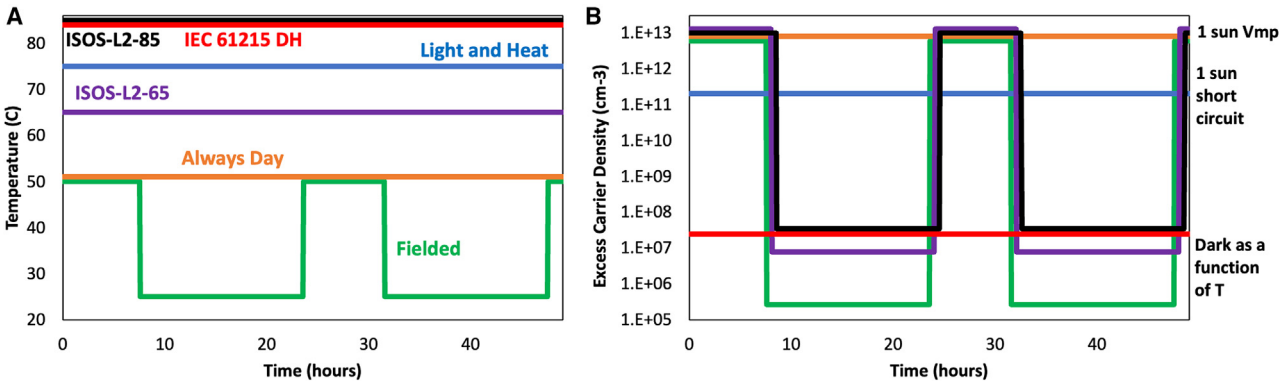

Figure 3. Simulated test conditions

(A) Temperature and (B) excess carrier density as a function of time for the accelerated test conditions of Table 1.

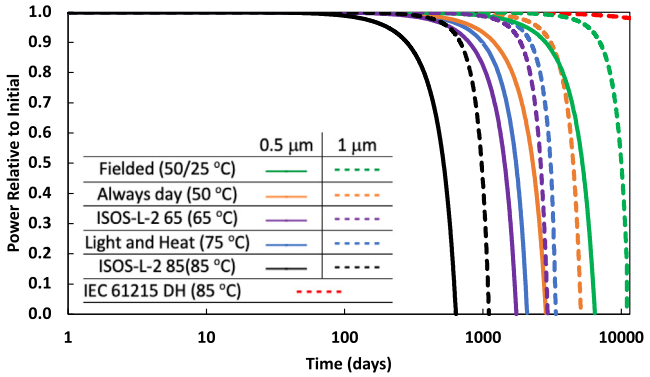

Figure 4. Simulated power output

Predicted evolution of power output under several test conditions for two different $MAPbI_3$ thicknesses.

has a modest effect on the degradation rate. The 75°C light and heat curve (blue) is swapped with the 65°C ISOS-L-2 65 curve (purple), compared to a temperature-only ordering. In other words, for an edge-sealed package under operating conditions, the availability of O_2 is the limiting factor in the DPO rate. Only for carrier densities well below operating conditions does the degradation rate depend on excess carrier density.

(5) The 0.5 µm absorber is expected to degrade to 80% performance after approximately 10 years (accounting for DPO only). However, even the most aggressive test on the 0.5 µm film will not produce measurable power degradation in less than 4 months. For a fielded module, the time to degrade to 80% performance will be less than those calculated here in the likely event that multiple degradation mechanisms (such as thermal decomposition or ion migration[16]) proceed in parallel.

Calculated degradation rates could be decreased via a variety of design changes, including wider edge seals, use of novel sealing techniques like laser welding, incorporation of an O_2 getter, or thicker $MAPbI_3$.

Some situations could cause degradation to occur more quickly than that shown in Figure 4. For example, packaging material is often saturated with O_2 during handling prior to module assembly, meaning that some O_2 will enter the absorber without needing to diffuse through the edge seal. Additionally, other degradation mechanisms may be less forgiving to the amount of O_2 ingress than that examined in this study. Consumption of a large fraction of the $MAPbI_3$ via photooxidation requires O_2 to act on the absorber in amounts similar to the molar density of the absorber itself, i.e., 10^{21} cm^{-3}. However, if O_2 can cause a deep electronic defect (e.g., Meng et al.[78]), or degrade a critical interface, a much lower amount of O_2 (e.g., 10^{15} cm^{-3}) could create a large decrease in performance. Also, multiple degradation mechanisms typically occur in parallel.[18]

Packaging controls photooxidation rate

Simulations described below indicate that DPO of $MAPbI_3$ is limited by how fast O_2 can flow into the module package, not by how fast an accumulation of O_2 reacts with the $MAPbI_3$. In DPO of $MAPbI_3$, each mole of O_2 consumes 4 mol of $MAPbI_3$.[46,69] Thus, at long timescales (i.e., much longer than the lag times), if the limiting process is diffusion through the PIB, then the moles of photooxidized $MAPbI_3$ will equal

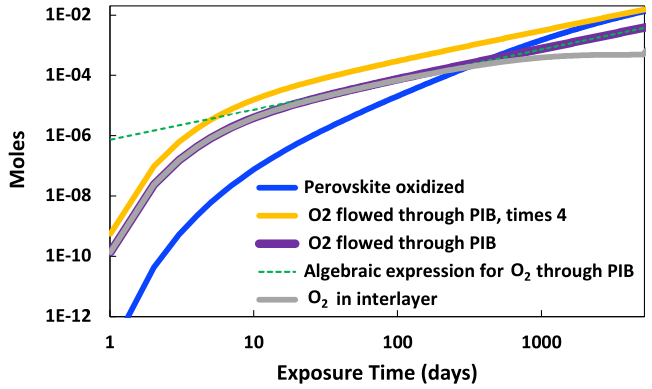

Figure 5. Cumulative O_2 flow calculations

Simulation output showing various O_2-related amounts for a packaged 1 μm $MAPbI_3$ film at 50°C.

about four times the amount of O_2 that has diffused through the PIB. Calculations related to moles of O_2 diffused and perovskite reacted are shown in Figure 5. Figure 5 is calculated using the always-day conditions defined in Figure 3, but the conclusion that packaging limits the degradation rate holds true for all test conditions examined in this work. The blue line (moles $MAPbI_3$ consumed) converges with the yellow line (4× moles O_2 through the PIB) after approximately 1,000 days. Furthermore, for a fast reaction, O_2 in the module interior is depleted to a low pressure, and the O_2 flow through the PIB can be approximated by a solution to the diffusion equation that has a fixed O_2 concentration on the atmosphere side of the PIB and none inside the package (Equation 4.4 in Crank[55]). The flow through the barrier is given by

$$\text{flow} = \frac{D\,C\,A_{\perp}}{L} = 7.2 \times 10^{-7} \text{moles per day} \qquad \text{(Equation 14)}$$

for the PIB edge seal of Figure 1. $A_{\perp}$ is the area perpendicular to O_2 flow (PIB thickness × module perimeter) and L is the length parallel to O_2 flow (i.e., the 1 cm edge seal width). This algebraic approximation appears in Figure 4 as a dotted green line and provides a good long-term estimate of the amount of O_2 that has flowed through the PIB and thus the reaction rate. At short timescales, the algebraic expression does not agree well, as it does not account for solubility-related lag time.

Because diffusion through the PIB is the rate-limiting step, the simulation results are not very sensitive to approximations of the lesser-known quantities in the reaction rate, such as excess carrier density at maximum power point.

As described in the experimental procedures, our results rely on the simplifying assumption of uniform O_2 distribution in the interlayer. This assumption is violated in the case of full-size modules with a polyolefin elastomer (POE) interlayer. In such modules, photooxidation near the edge of the modules (~10 cm) is expected to proceed similarly to our results, and this remains a substantial degradation concern. Diffusion through the edge seal remains the rate-limiting step even for full-sized modules with a POE interlayer.

Implications for thin-film cell barriers

Incorporating a barrier into unpackaged MHP devices has been observed to dramatically improve longevity in accelerated tests.[79–82] Such barriers block diffusion perpendicular to the MHP absorber layer. They are placed on the non-glass side of the MHP and block diffusion directly from the atmosphere in an unpackaged device or from the interlayer in a packaged device. The geometric factors in Equation 14

Table 2. Measured WVTRs for three examples of advanced barrier coatings

Barrier	Measurement temperature for WVTR (°C)	WVTR (g/m^2/day)	Implied O_2 flow into the module (moles/day)
Atomic layer deposition of SnO_x[85]	70	3×10^{-6}	3×10^{-7}
Atomic layer deposition of stack: 1 cycle Al_2O_3 + 4 cycles ZnO[86]	85	6×10^{-6}	6×10^{-7}
Commercial multi-layer product, materials and deposition techniques not specified[84]	50	6×10^{-5}	7×10^{-6}

Results in the rightmost column should be compared to a maximum rate of 7.2×10^{-7} mol per day derived for permeation through an edge seal.

imply that, for gases diffusing into the device stack, such barriers will improve test results on bare devices but are not likely to strongly improve the long-term behavior of modules with edge seals. For example, for the PIB of Figure 1, the geometric factors in Equation 14 are

$$\frac{A_{\perp,PIB}}{L_{PIB}} = \frac{450\ \mu m \times 6\ m}{1\ cm} = 0.27\ m. \qquad \text{(Equation 15)}$$

In contrast, for a thin-film cell barrier, assuming a maximum barrier thickness similar to that of the interlayer,

$$\frac{A_{\perp,cell-top}}{L_{cell-top}} = \frac{2 \times 1\ m}{<450\ \mu m} > 4,400\ m. \qquad \text{(Equation 16)}$$

Thus, for similar barrier material diffusivities, the flow will be more than 10,000 times faster through the thin-film cell barrier than through the edge seal. In practice, thin-film cell barrier layers coated directly onto the cell may be substantially thinner than the 450 μm assumed in Equation 16, causing an even large geometry-related difference between the impact of the edge seal versus that of the cell barrier.

Incorporating measured diffusion properties in the comparison of thin-film cell barriers and edge seals can provide further insight. Examples of some of the lowest WVTRs reported for research-sized[83] and commercial[84] barrier films are shown in Table 2. The implied daily flow of O_2 into a 2 m^2 module is calculated in the last column, assuming that the diffusivity of O_2 is similar to that of H_2O. The value in the last column can be compared with 7.2×10^{-7} mol per day derived for the edge seal in Equation 14 and Figure 5. Even the best research-sized coatings limit O_2 flow only to a similar magnitude as the edge seal. Furthermore, for PVs, taking advantage of the low WVTRs achieved in the research-size samples will require the difficult task of nearly eliminating localized defects like pinholes in the barrier over square meters of area.

The calculations of this section do not consider barriers that are meant to keep volatile absorber constituents trapped[87] within the solar cell.

In summary, this work illustrates the application of a physics and chemistry of failure approach to calculating AFs for MHP modules. Such AFs can help build confidence for a robust market despite a short product history. Product degradation is predicted by integrating accelerated tests with understanding of the degradation mechanisms. While this paper performs such predictions for one degradation mechanism, the physics and chemistry of failure approach can be applied more widely as degradation mechanisms for new cell and module types are identified and degradation kinetics are quantified.

A two-step physical model, including O_2 diffusion and the photooxidation of $MAPbI_3$, was developed. Temperatures and carrier densities encountered during

commonly used module accelerated stress tests or fielded conditions were input to the model. The following results were found:

(1) AFs are low, and these tests are thus only useful to screen for early failures, not to probe decades of performance potentially impacted by photooxidation of $MAPbI_3$.
(2) Dark damp heat tests are not expected to accelerate the primary degradation mode for $MAPbI_3$.
(3) Even the most aggressive test considered will not produce measurable power degradation from DPO in less than 4 months. Fielded modules, on the other hand, will degrade within the desired 20–30 year product lifetime. For example, a module with a 0.5 μm $MAPbI_3$ absorber and a 1 cm edge seal is expected to degrade to 80% performance after approximately 10 years under fielded conditions.
(4) Actual degradation rates will be larger than those calculated, in the likely event that multiple degradation mechanisms proceed in parallel.
(5) Module design choices, such as edge seal width or absorber thickness, will affect the degradation rate.
(6) Degradation mechanisms that form an active electronic defect with O_2 exposure are likely to cause power loss at lower O_2 concentrations and thus shorter time periods than DPO.
(7) Diffusion of O_2 into the package is shown to be the limiting step in the photooxidation rate of $MAPbI_3$.
(8) Due to package geometry, thin-film barriers coated onto the solar cell may dramatically improve test results on bare devices but are unlikely to markedly decrease the diffusion of gas to the absorber when using an edge-sealed package.

EXPERIMENTAL PROCEDURES

Resource availability

Lead contact

Further information and requests for resources should be directed to the lead contact, Ingrid Repins (ingrid.repins@nrel.gov).

Materials availability

This paper did not generate new materials.

Data and code availability

The data and code supporting this study are available from the corresponding author upon reasonable request.

SUPPLEMENTAL INFORMATION

Supplemental information can be found online at https://doi.org/10.1016/j.xcrp.2024.101969.

ACKNOWLEDGMENTS

This work was authored by the National Renewable Energy Laboratory, operated by the Alliance for Sustainable Energy, LLC, for the US Department of Energy (DOE) under contract no. DE-AC36-08GO28308. Funding was provided by the US DOE Office of Energy Efficiency and Renewable Energy (EERE) under Solar Energy Technologies Office (SETO) agreement no. 38050. The views expressed in the article do not necessarily represent the views of the DOE or the US government. The US

AUTHOR CONTRIBUTIONS

I.L.R. conceived of the study and performed calculations. All authors contributed to background and numerical inputs for the study, in particular: J.J.B. and L.T.S. for perovskite properties and degradation mechanisms, N.Y.D. and M.D.K. for module packaging, and M.O.-B., M.G.D., and T.J.S. for the perovskite accelerated test and performance. All authors contributed to writing, reviewing, and editing the manuscript.

DECLARATION OF INTERESTS

The authors declare no competing interests.

Received: November 27, 2023
Revised: March 15, 2024
Accepted: April 17, 2024
Published: May 7, 2024

REFERENCES

1. Ayre, J. (2016). Lux Research: Perovskite Solar Cells Technology Improving, Commercialization Likely in 2019. CleanTechnical. https://cleantechnica.com/2016/05/16/lux-research-perovskite-solar-cells-technology-improving-commercialization-likely-2019/.

2. Service, R.F. (2016). Low-cost solar cells poised for commercial breakthrough. Science.org. https://www.science.org/content/article/low-cost-solar-cells-poised-commercial-breakthrough.

3. Ford, N. (2023). Perovskite solar goes commercial as yield gains align with market forces. Reuters. https://www.reuters.com/business/energy/perovskite-solar-goes-commercial-yield-gains-align-with-market-forces-2023-02-02/.

4. Perovskites take steps to industrialization (2020). Nat. Energy *5*, 1. https://doi.org/10.1038/s41560-020-0552-6.

5. Kumagai, J. (2019). Power from commercial perovskit solar cells is coming soon. IEEE Spectr. https://spectrum.ieee.org/power-from-commercial-perovskite-solar-cells-is-coming-soon.

6. Stoker, L. (2020). Solar Perovskite Start-Up Evolar Bags New Investment to Target Rapid Commercialisation. PVTech. https://www.pv-tech.org/solar-perovskite-start-up-evolar-bags-new-investment-to-target-rapid-commercialisation/.

7. Wilson, I. (2019). Solar's Hot New Thing Nears Production. Q&A. BloombergNEF7. https://about.bnef.com/blog/solars-hot-new-thing-nears-production-qa/.

8. Siegler, T.D., Dawson, A., Lobaccaro, P., Ung, D., Beck, M.E., Nilsen, G., and Tinker, L.L. (2022). The Path to Perovskite Commercialization: A Perspective from the United States Solar Energy Technologies Office. ACS Energy Lett. *7*, 1728–1734. https://doi.org/10.1021/acsenergylett.2c00698.

9. Jordan, D.C., Haegel, N., and Barnes, T.M. (2022). Photovoltaics module reliability for the terawatt age. Prog. Energy *4*, 22002. https://doi.org/10.1088/2516-1083/ac6111.

10. Snaith, H.J., and Hacke, P. (2018). Enabling reliability assessments of pre-commercial perovskite photovoltaics with lessons learned from industrial standards. Nat. Energy *3*, 459–465. https://doi.org/10.1038/s41560-018-0174-4.

11. Christians, J.A., Habisreutinger, S.N., Berry, J.J., and Luther, J.M. (2018). Stability in Perovskite Photovoltaics: A Paradigm for Newfangled Technologies. ACS Energy Lett. *3*, 2136–2143. https://doi.org/10.1021/acsenergylett.8b00914.

12. Zhou, H., Chen, Q., Li, G., Luo, S., Song, T.b., Duan, H.-S., Hong, Z., You, J., Liu, Y., and Yang, Y. (2014). Interface engineering of highly efficient perovskite solar cells. Science *345*, 542–546. https://doi.org/10.1126/science.1254050.

13. Yang, J., Siempelkamp, B.D., Liu, D., and Kelly, T.L. (2015). Investigation of CH3NH3PbI3 Degradation Rates and Mechanisms in Controlled Humidity Environments Using in Situ Techniques. ACS Nano *9*, 1955–1963. https://doi.org/10.1021/nn506864k.

14. Bryant, D., Aristidou, N., Pont, S., Sanchez-Molina, I., Chotchunangatchaval, T., Wheeler, S., Durrant, J.R., and Haque, S.A. (2016). Light and oxygen induced degradation limits the operational stability of methylammonium lead triiodide perovskite solar cells. Energy Environ. Sci. *9*, 1655–1660. https://doi.org/10.1039/c6ee00409a.

15. Zhao, X., Liu, T., Burlingame, Q.C., Liu, T., Holley, R., Cheng, G., Yao, N., Gao, F., and Loo, Y.-L. (2022). Accelerated aging of all-inorganic, interface-stabilized perovskite solar cells. Science *377*, 307–310. https://doi.org/10.1126/science.abn5679.

16. Fu, W., Ricciardulli, A.G., Akkerman, Q.A., John, R.A., Tavakoli, M.M., Essig, S., Kovalenko, M.V., and Saliba, M. (2022). Stability of perovskite materials and devices. Mater. Today *58*, 275–296. https://doi.org/10.1016/j.mattod.2022.06.020.

17. Raman, R.K., Gurusamy Thangavelu, S.A., Venkataraj, S., and Krishnamoorthy, A. (2021). Materials, methods and strategies for encapsulation of perovskite solar cells: From past to present. Renew. Sustain. Energy Rev. *151*, 111608. https://doi.org/10.1016/j.rser.2021.111608.

18. Wang, Y., Arumugam, G.M., Mahmoudi, T., Mai, Y., and Hahn, Y.-B. (2021). A critical review of materials innovation and interface stabilization for efficient and stable perovskite photovoltaics. Nano Energy *87*, 106141. https://doi.org/10.1016/j.nanoen.2021.106141.

19. Osterwald, C.R., and McMahon, T.J. (2009). History of accelerated and qualification testing of terrestrial photovoltaic modules: A literature review. Progress in Photovoltaics. *17*, 11–33. https://doi.org/10.1002/pip.861.

20. Ross, J., R.G., and Smokler, M.I. (1986). Flat-Plate Solar Array Project Final Report (JPL). https://www.osti.gov/biblio/6802984.

21. Smokler, M.I., Otth, D.H., and Ross, J.,R.G. (1985). BLOCK PROGRAM APPROACH TO PHOTOVOLTAIC MODULE DEVELOPMENT, pp. 1150–1158.

22. Jordan, D.C., Repins, I.L., Kempe, M.D., Bleem, J., Menard, J., and Davis, P. (2021). Life after 30

Years: A PV System in Colorado. https://www.nrel.gov/docs/fy23osti/79039.pdf.

23. Virtuani, A., Caccivio, M., Annigoni, E., Friesen, G., Chianese, D., Ballif, C., and Sample, T. (2019). 35 years of photovoltaics: Analysis of the TISO-10-kW solar plant, lessons learnt in safety and performance—Part 1. Progress in Photovoltaics. *27*, 328–339. https://doi.org/10.1002/pip.3104.

24. Annigoni, E., Virtuani, A., Caccivio, M., Friesen, G., Chianese, D., and Ballif, C. (2019). 35 years of photovoltaics: Analysis of the TISO-10-kW solar plant, lessons learnt in safety and performance—Part 2. Progress in Photovoltaics. *27*, 760–778. https://doi.org/10.1002/pip.3146.

25. Jordan, D.C., Kurtz, S.R., VanSant, K., and Newmiller, J. (2016). Compendium of photovoltaic degradation rates. Progress in Photovoltaics. *24*, 978–989. https://doi.org/10.1002/pip.2744.

26. Jones-Albertus, R., Feldman, D., Fu, R., Horowitz, K., and Woodhouse, M. (2016). Technology advances needed for photovoltaics to achieve widespread grid price parity. Progress in Photovoltaics. *24*, 1272–1283. https://doi.org/10.1002/pip.2755.

27. Peters, I.M., Hauch, J., Brabec, C., and Sinha, P. (2021). The value of stability in photovoltaics. Joule *5*, 3137–3153. https://doi.org/10.1016/j.joule.2021.10.019.

28. Zhang, D., Li, D., Hu, Y., Mei, A., and Han, H. (2022). Degradation pathways in perovskite solar cells and how to meet international standards. Commun. Mater. *3*, 58. https://doi.org/10.1038/s43246-022-00281-z.

29. Shi, L., Bucknall, M.P., Young, T.L., Zhang, M., Hu, L., Bing, J., Lee, D.S., Kim, J., Wu, T., Takamure, N., et al. (2020). Gas chromatography–mass spectrometry analyses of encapsulated stable perovskite solar cells. Science *368*, eaba2412. https://doi.org/10.1126/science.aba2412.

30. Bogachuk, D., Saddedine, K., Martineau, D., Narbey, S., Verma, A., Gebhardt, P., Herterich, J.P., Glissmann, N., Zouhair, S., Markert, J., et al. (2022). Perovskite Photovoltaic Devices with Carbon-Based Electrodes Withstanding Reverse-Bias Voltages up to –9 V and Surpassing IEC 61215:2016 International Standard. Sol. RRL *6*, 2100527. https://doi.org/10.1002/solr.202100527.

31. Mei, A., Sheng, Y., Ming, Y., Hu, Y., Rong, Y., Zhang, W., Luo, S., Na, G., Tian, C., Hou, X., et al. (2020). Stabilizing Perovskite Solar Cells to IEC61215:2016 Standards with over 9,000-h Operational Tracking. Joule *4*, 2646–2660. https://doi.org/10.1016/j.joule.2020.09.010.

32. New method allows perovskite solar cells to meet IEC testing requirements (2020). [Available at URL: https://www.iec.ch/blog/new-method-allows-perovskite-solar-cells-meet-iec-testing-requirements.]

33. Hacke, P., Smith, R., Terwilliger, K., Glick, S., Jordan, D., Johnston, S., Kempe, M., and Kurtz, S. (2013). Acceleration factor determination for potential-induced degradation in crystalline silicon PV modules. 4B.1.1-4B.1.5. https://doi.org/10.1109/IRPS.2013.6532009.

34. Lechner, P., Schnepf, J., and Stellbogen, D. (2017). Performance Characterisation and Extended Reliability Testing of CIGS PV Modules, pp. 1004–1009.

35. Pescetelli, S., Agresti, A., Viskadouros, G., Razza, S., Rogdakis, K., Kalogerakis, I., Spiliarotis, E., Leonardi, E., Mariani, P., Sorbello, L., et al. (2022). Integration of two-dimensional materials-based perovskite solar panels into a stand-alone solar farm. Nat. Energy *7*, 597–607. https://doi.org/10.1038/s41560-022-01035-4.

36. Paraskeva, V., Hadjipanayi, M., Norton, M., Aguirre, A., Hadipour, A., Song, W., Fontanot, T., Christiansen, S., Ebner, R., and Georghiou, G.E. (2023). Long-Term Outdoor Testing of Perovskite Mini-Modules: Effects of FACl Additives. Energies *16*, 2608. https://doi.org/10.3390/en16062608.

37. Paraskeva, V., Hadjipanayi, M., Norton, M., Aguirre, A., Hadipour, A., Ebner, R., and Georghiou, G.E. (2022). Seasonal dependence of diurnal efficiency degradation and recovery in perovskite mini-modules during outdoor testing, pp. 217–222. https://doi.org/10.1109/PVSC48317.2022.9938726.

38. Babics, M., De Bastiani, M., Ugur, E., Xu, L., Bristow, H., Toniolo, F., Raja, W., Subbiah, A.S., Liu, J., Torres Merino, L.V., et al. (2023). One-year outdoor operation of monolithic perovskite/silicon tandem solar cells. Cell Rep. Phys. Sci. *4*, 101280. https://doi.org/10.1016/j.xcrp.2023.101280.

39. Aime, G., Ciocia, A., Malgaroli, G., Narbey, S., Saglietti, L., and Spertino, F. (2023). Degradation Assessment for Prototypal Perovskite Photovoltaic Modules in Long Term Outdoor Experimental Campaign. https://doi.org/10.1109/EEEIC/ICPSEurope57605.2023.10194854.

40. Emery, Q., Remec, M., Paramasivam, G., Janke, S., Dagar, J., Ulbrich, C., Schlatmann, R., Stannowski, B., Unger, E., and Khenkin, M. (2022). Encapsulation and Outdoor Testing of Perovskite Solar Cells: Comparing Industrially Relevant Process with a Simplified Lab Procedure. ACS Appl. Mater. Interfaces *14*, 5159–5167. https://doi.org/10.1021/acsami.1c14720.

41. De Bastiani, M., Van Kerschaver, E., Jeangros, Q., Ur Rehman, A., Aydin, E., Isikgor, F.H., Mirabelli, A.J., Babics, M., Liu, J., Zhumagali, S., et al. (2021). Toward Stable Monolithic Perovskite/Silicon Tandem Photovoltaics: A Six-Month Outdoor Performance Study in a Hot and Humid Climate. ACS Energy Lett. *6*, 2944–2951. https://doi.org/10.1021/acsenergylett.1c01018.

42. Topic, M., Lipovsek, B., Glazar, B., Brecl, K., Albrecht, S., and Jost, M. (2020). From the lab to roof top applications: Outdoor performance, temperature behavior and energy yield of perovskite solar cells, pp. 599–602. https://doi.org/10.1109/PVSC45281.2020.9300419.

43. Jiang, Q., Tirawat, R., Kerner, R.A., Gaulding, E.A., Xian, Y., Wang, X., Newkirk, J.M., Yan, Y., Berry, J.J., and Zhu, K. (2023). Towards linking lab and field lifetimes of perovskite solar cells. Nature *623*, 313–318. https://doi.org/10.1038/s41586-023-06610-7.

44. Eaton, D.H., Durrant, N., Huber, S.J., Blish, R., and Lycoudes, N. (2000). Knowledge-Based Reliability Qualification Testing of Silicon Devices. (SEMATECH).

45. Challa, V., Rundle, P., and Pecht, M. (2013). Challenges in the qualification of electronic components and systems. IEEE Trans. Device Mater. Reliab. *13*, 26–35. https://doi.org/10.1109/TDMR.2011.2173801.

46. Siegler, T.D., Dunlap-Shohl, W.A., Meng, Y., Yang, Y., Kau, W.F., Sunkari, P.P., Tsai, C.E., Armstrong, Z.J., Chen, Y.-C., Beck, D.A.C., et al. (2022). Water-Accelerated Photooxidation of CH3NH3PbI3Perovskite. J. Am. Chem. Soc. *144*, 5552–5561. https://doi.org/10.1021/jacs.2c00391.

47. Kempe, M.D., Dameron, A.A., Moricone, T.J., and Reese, M.O. (2010). Evaluation and modeling of edge-seal materials for photovoltaic applications, pp. 256–261. https://doi.org/10.1109/PVSC.2010.5614463.

48. Kempe, M.D., Dameron, A.A., and Reese, M.O. (2014). Evaluation of moisture ingress from the perimeter of photovoltaic modules. Progress in Photovoltaics. *22*, 1159–1171. https://doi.org/10.1002/pip.2374.

49. Kempe, M.D., Panchagade, D., Reese, M.O., and Dameron, A.A. (2015). Modeling moisture ingress through polyisobutylene-based edge-seals. Progress in Photovoltaics. *23*, 570–581. https://doi.org/10.1002/pip.2465.

50. Kempe, M.D., Nobles, D.L., Postak, L., and Calderon, J.A. (2018). Moisture ingress prediction in polyisobutylene-based edge seal with molecular sieve desiccant. Progress in Photovoltaics. *26*, 93–101. https://doi.org/10.1002/pip.2947.

51. Cahen, D., and Noufi, R. (1989). Defect chemical explanation for the effect of air anneal on CdS/CuInSe 2 solar cell performance. Appl. Phys. Lett. *54*, 558–560. https://doi.org/10.1063/1.100930.

52. Zhao, H., Farah, A., Morel, D., and Ferekides, C.S. (2009). The effect of impurities on the doping and VOC of CdTe/CdS thin film solar cells. Thin Solid Films *517*, 2365–2369. https://doi.org/10.1016/j.tsf.2008.11.041.

53. Van Amerongen, G.J. (1946). The permeability of different rubbers to gases and its relation to diffusivity and solubility. J. Appl. Phys. *17*, 972–985. https://doi.org/10.1063/1.1707667.

54. Strevel, N., Trippel, L., Kotarba, C., and Khan, I. (2013). Improvements in CdTe module reliability and long-term degradation through advances in construction and device innovation. Photovolt. Int. *22*. https://www.pv-tech.org/technical-papers/improvements-in-cdte-module-reliability-and-longterm-degradation-through-advances-in-construction-and-device-innovation/.

55. Crank, J. (1975). The Mathematics of Diffusion, 2d ed. (Clarendon Press).

56. Xie, B., Fan, X.J., Shi, X.Q., and Ding, H. (2009). Direct concentration approach of moisture diffusion and whole-field vapor pressure modeling for reflow process-part I: Theory and numerical implementation. J. Electron. Packag. *131*, 310101–310107. https://doi.org/10.1115/1.3144147.

57. Kapur, J., Norwood, J.L., and Cwalina, C.D. (2013). Determination of Moisture Ingress Rate through Photovoltaic Encapsulants, pp. 3020–3023. https://doi.org/10.1109/PVSC.2013.6745097.

58. Wisniewski, D., Lv, R., Nair, S.V., Jaubert, J.-N., Xu, T., and Ruda, H.E. (2019). Measurement and modelling of water ingress into double-glass photovoltaic modules. Progress in Photovoltaics. *27*, 144–151. https://doi.org/10.1002/pip.3069.

59. Suzuki, A., Takahagi, H., Uehigashi, A., and Hara, S. (2015). Development of reliable technique for evaluating the properties of water vapor barriers. AIP Adv. *5*, 117204. https://doi.org/10.1063/1.4935341.

60. Graff, G.L., Williford, R.E., and Burrows, P.E. (2004). Mechanisms of vapor permeation through multilayer barrier films: Lag time versus equilibrium permeation. J. Appl. Phys. *96*, 1840–1849. https://doi.org/10.1063/1.1768610.

61. Lauvray, H., Einhaus, R., Baret, G., and Bamberg, K. (2008). Photovoltaic Module and Method for Production Thereof. US patent 20080257401A1. published October 23, 2008.

62. Ellis, S., Maple, L., Shimpi, T., Pavgi, A., Tamizhmani, G., Sampth, W., and Barth, K. (2021). Reliability and Manufacturing Demonstrations of a New Photovoltaic Module Architecture and Streamlined Approach to Encpasulation, pp. 1504–1506. https://doi.org/10.1109/PVSC43889.2021.9518523.

63. Jaysankar, M., Filipič, M., Zielinski, B., Schmager, R., Song, W., Qiu, W., Paetzold, U.W., Aernouts, T., Debucquoy, M., Gehlhaar, R., and Poortmans, J. (2018). Perovskite-silicon tandem solar modules with optimised light harvesting. Energy Environ. Sci. *11*, 1489–1498. https://doi.org/10.1039/c8ee00237a.

64. Welty, J., Rorrer, G.L., and Foster, D.G. (2015). Fundamentals of Momentum, Heat, and Mass Transfer Sixth (Wiley).

65. Marais, S., Saiter, J.M., Devallencourt, C., Nguyen, Q.T., and Métayer, M. (2002). Study of transport of small molecules through ethylene-co-vinyl acetate copolymers films. Part B: CO2 and O2 gases. Polym. Test. *21*, 425–431. https://doi.org/10.1016/S0142-9418(01)00106-4.

66. Seguchi, T., and Yamomoto, Y. (1986). Diffusion and Solubility of Oxygen in Gamma Ray Irradiated Polymer Insulation Materials (Japan Atomic Energy Research Institute).

67. Toniolo, F., Bristow, H., Babics, M., Loiola, L.M.D., Liu, J., Said, A.A., Xu, L., Aydin, E., Allen, T.G., Meneghetti, M., et al. (2023). Efficient and reliable encapsulation for perovskite/silicon tandem solar modules. Nanoscale *15*, 16984–16991. https://doi.org/10.1039/D2NR06873G.

68. Cheacharoen, R., Boyd, C.C., Burkhard, G.F., Leijtens, T., Raiford, J.A., Bush, K.A., Bent, S.F., and McGehee, M.D. (2018). Encapsulating perovskite solar cells to withstand damp heat and thermal cycling. Sustain. Energy Fuels *2*, 2398–2406. https://doi.org/10.1039/C8SE00250A.

69. Aristidou, N., Eames, C., Sanchez-Molina, I., Bu, X., Kosco, J., Islam, M.S., and Haque, S.A. (2017). Fast oxygen diffusion and iodide defects mediate oxygen-induced degradation of perovskite solar cells. Nat. Commun. *8*, 15218. https://doi.org/10.1038/ncomms15218.

70. Aristidou, N., Sanchez-Molina, I., Chotchuangchutchaval, T., Brown, M., Martinez, L., Rath, T., and Haque, S.A. (2015). The Role of Oxygen in the Degradation of Methylammonium Lead Trihalide Perovskite Photoactive Layers. Angew. Chem. Int. Ed. *54*, 8208–8212. https://doi.org/10.1002/anie.201503153.

71. Nagel, H., Berge, C., and Aberle, A.G. (1999). Generalized analysis of quasi-steady-state and quasi-transient measurements of carrier lifetimes in semiconductors. J. Appl. Phys. *86*, 6218–6221. https://doi.org/10.1063/1.371633.

72. Dunlap-Shohl, W.A., Meng, Y., Sunkari, P.P., Beck., D.A.C., Meilă, M., and Hillhouse, H.W. (2024). Physiochemical Machine Learning Models Predict Operational Lifetimes of CH3NH3PbI3 Perovskite Solar Cells. J. Mater. Chem. A *12*, 9730–9746. https://doi.org/10.1039/D3TA06668A.

73. Phillips, L.J., Rashed, A.M., Treharne, R.E., Kay, J., Yates, P., Mitrovic, I.Z., Weerakkody, A., Hall, S., and Durose, K. (2016). Maximizing the optical performance of planar CH3NH3PbI3 hybrid perovskite heterojunction stacks. Sol. Energy Mater. Sol. Cells *147*, 327–333. https://doi.org/10.1016/j.solmat.2015.10.007.

74. Schelhas, L., and Stein, J. (2022). PACT Perovskite PV Module Stress Testing Protocol. https://doi.org/10.2172/1843653. Version 0.0.

75. Khenkin, M.V., Katz, E.A., Abate, A., Bardizza, G., Berry, J.J., Brabec, C., Brunetti, F., Bulović, V., Burlingame, Q., Di Carlo, A., et al. (2020). Consensus statement for stability assessment and reporting for perovskite photovoltaics based on ISOS procedures. Nat. Energy *5*, 35–49. https://doi.org/10.1038/s41560-019-0529-5.

76. International Electrotechnical Commission (2021). IEC 61215-2 (2021). https://webstore.iec.ch/publication/61350.

77. Bosco, N., Silverman, T.J., and Kurtz, S. (2016). Climate specific thermomechanical fatigue of flat plate photovoltaic module solder joints. Microelectron. Reliab. *62*, 124–129. https://doi.org/10.1016/j.microrel.2016.03.024.

78. Meng, Y., Sunkari, P.P., Meilă, M., and Hillhouse, H.W. (2023). Chemical Reaction Kinetics of the Decomposition of Low-Bandgap Tin–Lead Halide Perovskite Films and the Effect on the Ambipolar Diffusion Length. ACS Energy Lett. *8*, 1688–1696. https://doi.org/10.1021/acsenergylett.2c02733.

79. Abdelmageed, G., Sully, H.R., Bonabi Naghadeh, S., El-Hag Ali, A., Carter, S.A., and Zhang, J.Z. (2018). Improved Stability of Organometal Halide Perovskite Films and Solar Cells toward Humidity via Surface Passivation with Oleic Acid. ACS Appl. Energy Mater. *1*, 387–392. https://doi.org/10.1021/acsaem.7b00069.

80. Koushik, D., Verhees, W.J.H., Kuang, Y., Veenstra, S., Zhang, D., Verheijen, M.A., Creatore, M., and Schropp, R.E.I. (2017). High-efficiency humidity-stable planar perovskite solar cells based on atomic layer architecture. Energy Environ. Sci. *10*, 91–100. https://doi.org/10.1039/c6ee02687g.

81. Zhang, J., Hu, Z., Huang, L., Yue, G., Liu, J., Lu, X., Hu, Z., Shang, M., Han, L., and Zhu, Y. (2015). Bifunctional alkyl chain barriers for efficient perovskite solar cells. Chem. Commun. *51*, 7047–7050. https://doi.org/10.1039/c5cc00128e.

82. Cao, J., Yin, J., Yuan, S., Zhao, Y., Li, J., and Zheng, N. (2015). Thiols as interfacial modifiers to enhance the performance and stability of perovskite solar cells. Nanoscale *7*, 9443–9447. https://doi.org/10.1039/c5nr01820j.

83. Jarvis, K.L., and Evans, P.J. (2017). Growth of thin barrier films on flexible polymer substrates by atomic layer deposition. Thin Solid Films *624*, 111–135. https://doi.org/10.1016/j.tsf.2016.12.055.

84. 3M (2018). Datasheet for 3M Ultra Barrier Solar Film 512. https://multimedia.3m.com/mws/media/1285470O/3m-ultra-barrier-solar-film-512.pdf.

85. Behrendt, A., Friedenberger, C., Gahlmann, T., Trost, S., Becker, T., Zilberberg, K., Polywka, A., Görrn, P., and Riedl, T. (2015). Highly Robust Transparent and Conductive Gas Diffusion Barriers Based on Tin Oxide. Adv. Mater. *27*, 5961–5967. https://doi.org/10.1002/adma.201502973.

86. Chou, C.-T., Yu, P.-W., Tseng, M.-H., Hsu, C.-C., Shyue, J.-J., Wang, C.-C., and Tsai, F.-Y. (2013). Transparent Conductive Gas-Permeation Barriers on Plastics by Atomic Layer Deposition. Adv. Mater. *25*, 1750–1754. https://doi.org/10.1002/adma.201204358.

87. Boyd, C.C., Cheacharoen, R., Bush, K.A., Prasanna, R., Leijtens, T., and McGehee, M.D. (2018). Barrier Design to Prevent Metal-Induced Degradation and Improve Thermal Stability in Perovskite Solar Cells. ACS Energy Lett. *3*, 1772–1778. https://doi.org/10.1021/acsenergylett.8b00926.